Majority and Minority Gates Realized in Enzyme-Biocatalyzed Systems Integrated with Logic Networks and Interfaced with Bioelectronic Systems

ARTICLE *in* THE JOURNAL OF PHYSICAL CHEMISTRY B · MAY 2014

Impact Factor: 3.3 · DOI: 10.1021/jp504057u · Source: PubMed

THE JOURNAL OF PHYSICAL CHEMISTRY B

Article

pubs.acs.org/JPCB

Majority and Minority Gates Realized in Enzyme-Biocatalyzed Systems Integrated with Logic Networks and Interfaced with Bioelectronic Systems

Shay Mailloux,[†] Nataliia Guz,[†] Andrey Zakharchenko,[‡] Sergiy Minko,[‡] and Evgeny Katz*,[†]

[†]Department of Chemistry and Biomolecular Science, Clarkson University, Potsdam, New York 13699-5810, United States

[‡]Nanostructured Materials Laboratory, University of Georgia, Athens, Georgia 30602, United States

Supporting Information

ABSTRACT: Biocatalytic reactions operating in parallel and resulting in reduction of NAD^+ or oxidation of NADH were used to mimic 3-input majority and minority logic gates, respectively. The substrates corresponding to the enzyme reactions were used as the input signals. When the input signals were applied at their high concentrations, defined as logic **1** input values, the corresponding biocatalytic reactions were activated, resulting in changes of the NADH concentration defined as the output signal. The NADH concentration changes were dependent on the number of parallel reactions activated by the input signals. The absence of the substrates, meaning their logic **0** input values, kept the reactions mute with no changes in the NADH concentration. In the system mimicking the majority function, the enzyme-biocatalyzed reactions resulted in a higher production of NADH when more than one input signal was applied at the logic **1** value. Another system mimicking the minority function consumed more NADH, thus leaving a smaller residual output signal, when more than one input signal was applied at the logic **1** value. The performance of the majority gate was improved by processing the output signal through a filter system in which another biocatalytic reaction consumed a fraction of the output signal, thus reducing its physical value to zero when the logic **0** value was obtained. The majority gate was integrated with a preceding AND logic gate to illustrate the possibility of complex networks. The output signal, NADH, was also used to activate a process mimicking drug release, thus illustrating the use of the majority gate in decision-making biomedical systems. The 3-input majority gate was also used as a switchable AND/OR gate when one of the input signals was reserved as a command signal, switching the logic operation for processing of the other two inputs. Overall, the designed majority and minority logic gates demonstrate novel functions of biomolecular information processing systems.

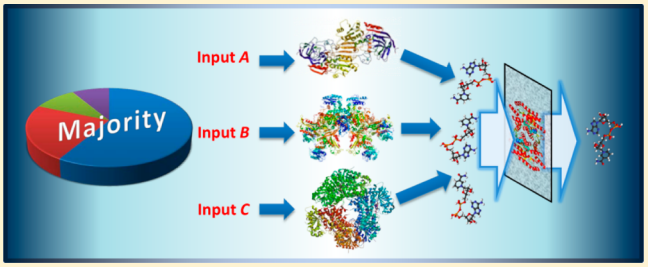

INTRODUCTION

Enzyme-based logic systems mimicking Boolean logic gates[1] represent a new facet in the general areas of molecular[2−7] and biomolecular[8−13] information processing. While computational applications of biomolecular systems[14−16] competing with modern electronics are rather futuristic, their use in low scale information processing for biosensing[17−19] and bioactuating,[20−22] particularly aiming at medical use[23−26] and operation in a biological environment,[27,28] is already feasible at the present level of technology. Rapid progress in enzyme-based information processing systems resulted in the design of biocatalytic cascades mimicking various Boolean logic gates,[1] including AND,[29−36] OR,[34,36,37] NAND,[38,39] NOR,[36,39] CNOT,[40] XOR,[34,36,41,42] INHIBIT,[34,36] Identity,[36] and Inverter[36] gates. Assembling enzyme logic gates in complex networks composed of several concatenated gates resulted in an increased complexity of the information processing systems.[43,44] Despite the fact that specific applications of the enzyme logic systems, for example for the analysis of injury biomarkers,[45,46] have already been formulated, the research is still in the process of filling a "toolbox" with various Boolean[1,29−44] and non-Boolean[47,48] components for future use. This research step is similar to the development of electronic elements in the mid-20th century, prior to the rapid progress in electronic and computing devices. The present paper reports new enzyme systems mimicking Boolean gates performing "majority" and "minority" logic operations. In Boolean logic, the circuit with the majority function returns true only when more than 50% of its inputs are true and false otherwise; the minority function operates in the opposite way, being the complement of the majority function.[49] While, in general, the majority and minority logic gates can operate with n input signals ($n > 2$), their simplest realization includes 3 inputs. Therefore, the 3-input majority gate generates the logic output **1** (true) when any two or all three inputs have logic values **1**, and otherwise, if more than one input has logic value

Received: April 25, 2014
Revised: May 28, 2014
Published: May 29, 2014

   dx.doi.org/10.1021/jp504057u | J. Phys. Chem. B 2014, 118, 6775−6784

0, the output is **0** (false). The 3-input minority gate generates the logic output **1** only when one or none of the inputs has a logic value of **1**, while any two or all inputs with the value **1** result in output **0**. These logic operations are considered highly important for electronic/computing systems.[49−52] Majority (voting) functions are used in fault-tolerant computing[53] and other applications, including synthesis of reversible logic circuits.[54] Overall, a 3-input majority gate is one of the most basic logic gates; on the molecular level, it can serve as a basic and versatile building block for constructing more complex circuits. However, until now, its biomolecular realization was reported in only two studies, both based on DNA biocomputing systems,[55,56] and never researched using enzymes. This new realization of majority and minority gates in enzyme-biocatalytic cascades allows their integration with enzyme logic networks, thus increasing the complexity of biomolecular information processing systems, allowing the switching between ON−OFF of various actuating functions when interfacing with electronics.

EXPERIMENTAL SECTION

Materials. Malate dehydrogenase (MDH; E.C. 1.1.1.37) from porcine heart, glucose-6-phosphate dehydrogenase (G6PDH; E.C. 1.1.1.49) from *Leuconostoc mesenteroides*, alcohol dehydrogenase (AlcDH; E.C. 1.1.1.1) from *Saccharomyces cerevisiae*, L-lactic dehydrogenase (LDH; E.C. 1.1.1.27) from porcine heart, glucose dehydrogenase (GDH; E.C. 1.1.1.47) from *Pseudomonas sp.*, diaphorase (Diaph; E.C. 1.8.1.4) from *Clostridium kluyveri*, esterase (Est; E.C. 3.1.1.1) from porcine liver, horseradish peroxidase (HRP; EC 1.11.1.7), β-nicotinamide adenine dinucleotide sodium salt (NAD^+), β-nicotinamide adenine dinucleotide reduced sodium salt (NADH), D-(+)-glucose (Glc), glucose-6-phosphate (Glc6P), ethanol (Et-OH), ethyl acetate (Et-Ac), oxaloacetic acid (Oxacet), methylene blue (MB), pyruvic acid (Pyr), sodium alginate from brown algae (medium viscosity, ≥2000 cP), pyrroloquinoline quinone (methoxatin disodium salt, PQQ), poly(ethylenimine) aqueous solution (PEI; average M_n 60 000), 3,3′,5,5′-tetramethylbenzidine dihydrochloride (TMB), (1-ethyl-3[3-(dimethylamino)propyl]carbodiimide (EDC), *N*-hydroxysuccimide (NHS), 2-amino-2-hydroxymethylpropane-1,3-diol (Tris-buffer), (4-(2-hydroxyethyl)-1-piperazineethanesulfonic acid (HEPES-buffer), rhodamine B isocyanate (RITC), 3-(aminopropyl)triethoxysilane (APS), tetraethyl orthosilicate (TEOS), and other standard organic and inorganic materials and reactants were obtained from Sigma-Aldrich or J.T. Baker and used without further purification. All experiments were carried out in ultrapure water (18.2 MΩ·cm; Barnstead NANOpure Diamond).

Instrumentation. A Shimadzu UV-2450 UV−vis spectrophotometer with 1 mL poly(methyl methacrylate) (PMMA) cuvettes were used for all optical kinetic measurements. A C1 Eclipse Nikon TE2000U fluorescent confocal microscope was used to collect all images. Electrochemical experiments were performed in a three-electrode cell: Metrohm Ag |AgCl|KCl, 3 M, reference, graphite counter, and graphite working electrode. A single compartment cell was used with an electrochemical workstation (ECO Chemie Autolab PASTAT 10) and GPES 4.9 (General Purpose Electrochemical System) software. All potentials are reported in the paper vs Ag |AgCl|KCl, 3 M reference electrode.

Experimental Procedures. *Operation of Majority Gate without Filter.* Glucose (input *A*, 2 mM for logic value **1**), glucose-6-phosphate (input *B*, 0.85 mM for logic value **1**), ethanol (input *C*, 21 mM for logic value **1**), GDH (1 U/mL), G6PDH (50 mU/mL), AlDH (4 U/mL), and NAD^+ (1.5 mM) were combined in Tris-HCl buffer (100 mM, pH 7.4) and used to generate NADH whose absorbance at 340 nm was monitored for 600 s. Logic values **0** for the inputs *A*, *B*, and *C* were defined as the absence of the corresponding chemicals.

Operation of Majority Gate with Filter. The above system was repeated in the presence of oxaloacetic acid (0.5 mM) and MDH (500 mU/mL).

Operation of Majority Gate with Filter and with Additional AND Gate. Glucose (input *A*, 2 mM for logic value **1**), glucose-6-phosphate (input *B*, 1.2 mM for logic value **1**), ethyl acetate (input *C*′, 10 mM for logic value **1**), esterase (input *C*″, 2.4 U/mL for logic value **1**), GDH (300 mU/mL), G6PDH (167 mU/mL), AlDH (4 U/mL), oxaloacetic acid (0.3 mM), MDH (400 mU/mL), and NAD^+ (1.5 mM) were combined in Tris-HCl buffer (500 mM, pH 7.4) and used to generate NADH whose absorbance at 340 nm was monitored for 600 s. Logic values **0** for the inputs *A*, *B*, *C*′, and *C*″ were defined as the absence of the corresponding chemicals.

Operation of Minority Gate. Oxaloacetic acid (input *A*, 150 μM for logic **1** value), methylene blue (input *B*, 105 μM for logic **1** value), pyruvic acid (input *C*, 100 μM for logic **1** value), MDH (15 mU/mL), LDH (10 mU/mL), diaphorase (250 mU/mL), and NADH (180 μM) were combined in Tris-HCl buffer (100 mM, pH 7.4) and used to consume NADH. A decrease in absorbance of NADH at 340 nm was monitored for 600 s.

Synthesis of Magnetic-Core Silica-Shell-Coated Nanoparticles Loaded with Rhodamine B and Their Functionalization with HRP. Magnetite (Fe_3O_4) nanoparticles were synthesized using the standard method[57] and then were coated with silica and encapsulated rhodamine B dye for fluorescent imaging. The detailed procedure is specified in the Supporting Information. Then, HRP was coupled to the APS amino-functionalities on the surface of the nanoparticles through a carbodiimide procedure: EDC (100 mM), NHS (100 mM), HRP (253 U), and 2 mg of the magnetic nanoparticles were combined in 1 mL of HEPES-buffer (10 mM, pH 7.5) and allowed to incubate for 3 h at room temperature while shaking. The HRP-functionalized nanoparticles were then washed and rebuffered three times in HEPES buffer (10 mM, pH 7.5).

Deposition of Alginate on a Graphite Electrode. Sodium alginate (1.5% w/w) was dissolved in 100 mM Na_2SO_4 (pH 6.0) and stirred for 30 min at 45 °C. The solution was cooled to room temperature; then, $FeSO_4$ (35 mM) and HRP-functionalized nanoparticles (NPs) (1 mg) were added and mixed well. The NPs were entrapped into the Fe^{3+}-cross-linked alginate film upon its electrochemical deposition on the electrode surface. The polymer film was deposited on a graphite electrode (pencil rod; geometrical area of 0.6 cm^2)[58] upon oxidation of Fe^{2+} cations at the potential of +0.8 V applied with a potentiostat. The electrochemically produced Fe^{3+} cations resulted in an alginate cross-linked film on a graphite surface containing entrapped NPs. The alginate-modified electrode was washed thoroughly with water. A polymer film with a thickness of ca. 100 μm was obtained after 60 s of electrochemical deposition. Electrochemical characterization of the alginate-modified electrode was detailed elsewhere.[59]

Functionalization of the Graphite Electrode with PQQ. Graphite electrodes (pencil rods; geometrical area of 0.6 cm^2)

dx.doi.org/10.1021/jp504057u | J. Phys. Chem. B 2014, 118, 6775−6784

Scheme 1. General Composition of the Enzyme-Based 3-Input Majority Gate (Section B) with a Preceding AND Logic Gate (Section A), Following Filter Unit (Section C) and an Ending Molecular-Release System Activated by Biomolecular Signals (Section D)[a]

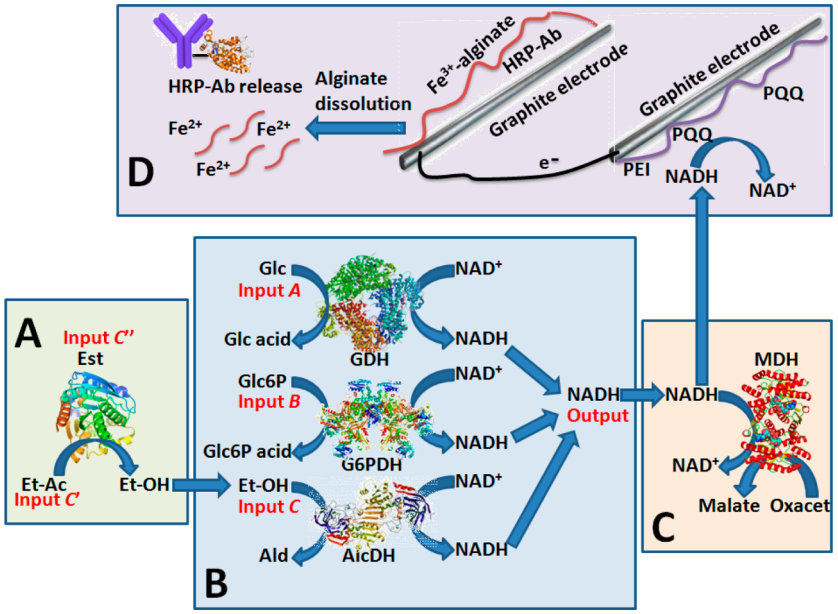

[a]The following abbreviations are used for the products of the biocatalytic reactions: Glc acid = gluconic acid, Glc6P acid = 6-phosphogluconic acid, Ald = acetaldehyde. All other abbreviations are explained in the text. The enzyme images are given for illustrating purposes only and may not correspond exactly to the used enzymes. Input signals *A*, *B*, and *C* are represented by glucose (Glc), glucose-6-phosphate (Glc6P), and ethanol (Et-OH), respectively. Additional input signals *C′* and *C″* are represented by ethyl acetate (Et-Ac) and esterase (Est).

were polished with sandpaper until appearing smooth and then were rinsed and incubated in 1% w/w PEI solution for 20 min. Following, the electrodes were washed three times with water and incubated in a solution containing EDC (50 mM), NHS (50 mM), and PQQ (20 μM) made in HEPES buffer (10 mM, pH 7.5) for 3 h. The electrodes were then washed and stored in HEPES buffer (10 mM, pH 7.5). The details of the PQQ immobilization procedure and the modified electrode characterization were reported elsewhere.[60]

Imaging of Entrapped NPs in Alginate. A C1 Eclipse Nikon TE2000U fluorescent confocal microscope was used to collect fluorescent images of NPs entrapped in a 100 μm thick alginate gel layer on a graphite electrode immersed in deionized water on a glass substrate; the alginate gel layer boundary can be clearly seen as a dark outline. A green laser with a wavelength of 543 nm was used for the fluorescent excitation of the Rhodamine B dye encapsulated in NPs. A 10× objective lens was used for imaging; the optical gains on the confocal microscope for both channels were 8.30, and the dwell time was 1.64 μs for all measurements.

RESULTS AND DISCUSSION

Scheme 1 shows the general composition of the enzyme-based 3-input majority gate (section B) with a preceding AND logic gate (section A), following filter unit (section C), and an ending molecular-release system activated by biomolecular signals (section D). Scheme 2 represents the chemical processes in terms of logic and actuation operations. The majority gate was realized with three reactions biocatalyzed by three NAD^+-dependent enzymes—glucose dehydrogenase (GDH), glucose-6-phosphate dehydrogenase (G6PDH), and alcohol dehydrogenase (AlcDH)—operating in parallel (Scheme 1B). The biocatalytic reactions were activated by

Scheme 2. Block Diagram Showing the Concatenated Logic Circuitry and the Ending Substance Releasing System[a]

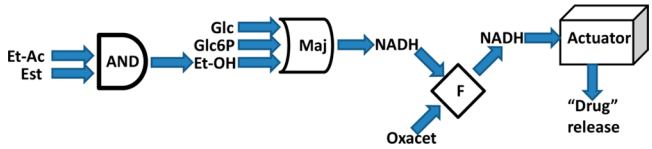

[a]The following abbreviations are used: Maj = majority gate, F = filter; all other abbreviations are explained in the text. Input signals are defined in Scheme 1 footnote.

input signals *A*, *B*, and *C*, represented by the corresponding substrates glucose (Glc), glucose-6-phosphate (Glc6P), and ethanol (Et-OH), respectively. Aiming at the simplest concept demonstration, logic value **0** for all input signals was defined as the absence of the substrates, while logic value **1** was defined as the experimentally convenient and optimized concentrations: 2 mM Glc, 0.85 mM Glc6P, and 21 mM Et-OH. All three reactions resulted in the generation of NADH upon reduction of the cofactor NAD^+ and concomitant oxidation of the substrate inputs. The NADH formation was followed by absorbance measurements at λ = 340 nm, which is typical for NADH analysis[61] (Figure 1A). As expected for the parallel operating biocatalytic reactions, the NADH production was increased with an increasing number of reactions contributing to the process. In other words, in the absence of all substrates (meaning logic **0** for all inputs), all three enzymes were mute, resulting in no production of NADH (Figure 1A, curve a). Applying any one of the three input signals (Glc, Glc6P, or Et-OH) at its logic **1** value resulted in the activation of one biocatalytic reaction, thus resulting in NADH production (Figure 1A, curves b–d). Note that the enzyme activities and

dx.doi.org/10.1021/jp504057u | J. Phys. Chem. B 2014, 118, 6775–6784

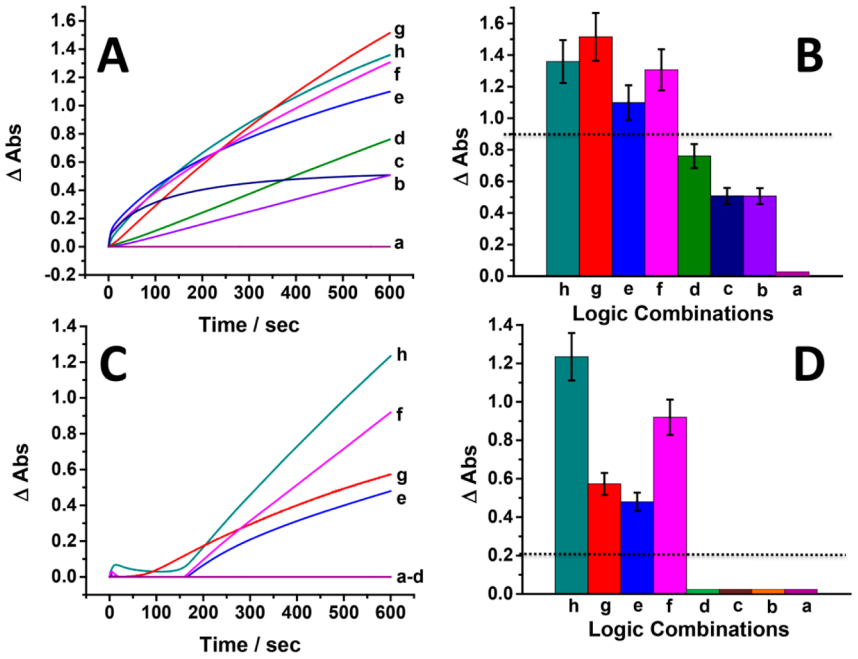

Figure 1. (A) Time-dependent absorbance changes corresponding to NADH production by the majority gate system activated by various combinations of the input signals. (B) Bar chart showing the optical absorbance of NADH measured at λ = 340 nm at the gate time of 600 s for various combinations of the input signals. (C) Time-dependent absorbance changes corresponding to NADH production by the majority gate system activated by various combinations of the input signals after processing the output signal through the filter. (D) Bar chart showing the optical absorbance of NADH measured at λ = 340 nm at the gate time of 600 s for various combinations of the input signals after processing the output signal through the filter. The input signal combinations were encoded in the following way: (a) **0**, **0**, **0**; (b) **0**, **1**, **0**; (c) **0**, **0**, **1**; (d) **1**, **0**, **0**; (e) **1**, **0**, **1**; (f) **0**, **1**, **1**; (g) **1**, **1**, **0**; (h) **1**, **1**, **1**. The input signals are shown in the flowing order: *A*, *B*, *C*. Input signals are defined in Scheme 1 footnote.

input concentrations were optimized to result in similar rates of NADH generation between all three biocatalytic processes. When two or all three inputs were applied at logic **1** values, the rate of the NADH production was increased due to parallel operation of two or three biocatalytic reactions (Figure 1A, curves e–h). The biocatalytically produced and optically measured NADH was considered as the output signal with the low and high concentrations defined as logic **0** and **1**, respectively, where logic **0** corresponds to no NADH production or NADH generation by any single pathway, while logic **1** corresponds to NADH production by any combination of two pathways or all three of them, following the definition of a majority gate.[49] While there is a clear difference between NADH production in one of the possible reaction pathways and in two/three of them operating simultaneously, the difference between physical values of logic **0** and **1** outputs is only ca. 2-fold at the gate time of 600 s (Figure 1B). The threshold separating **0** and **1** outputs is shown as a dashed line in Figure 1B.

Recent research aiming at reducing noise in the operation of enzyme-based logic gates resulted in the formulation of "filter" systems consuming a part of the output signal, thus bringing the output to physical zero when it is produced in small concentrations.[30−32,37,44] Applying this approach to the majority gate, we assembled a biocatalytic cascade partially consuming the produced NADH (Scheme 1C). Malate dehydrogenase (MDH) oxidized NADH produced by the reactions included in the majority gate with the concomitant reduction of oxaloacetate (Oxacet) to malate. It should be noted that MDH can reversibly catalyze the reaction in both directions.[62] Thus, accumulation of malate eventually pushes the opposite reaction to occur, finally resulting in a steady-state condition, limiting the extent of NADH oxidation.[63] The concentration of Oxacet was experimentally optimized to consume the entire amount of NADH produced by any single reaction pathway in the majority gate, thus bringing the logic **0** output to its physically zero level (Figure 1C, curves a–d). This resulted in much better separation between the logic **0** and **1** values of the output signal (Figure 1D). In other words, before the filtering process, the NADH concentrations (measured as optical absorbance at λ = 340 nm) corresponding to the logic output values **0** and **1** were different by ca. 2-fold, both being much above physical zero. When the filter reaction was applied, the NADH concentration corresponding to logic **0** became physically zero, while the concentration corresponding to logic **1** was significantly above zero. The threshold separating the **0** and **1** outputs is shown as a dashed line in Figure 1D. It should be noted that the mechanism of the filter operation is different from all previously studied biomolecular filters.[30−32,37,44] The mechanistic consideration and theoretical modeling of this filter operation will be reported elsewhere, being outside the scope of the present paper.

Outputs produced by biomolecular computing systems can be used to trigger chemical[64−66] and mechanical[22] actuation processes, for example, association/dissociation of nanoparticles,[67] inversion of an emulsion,[68] opening/closing of membrane pores,[69] restructuring of thin films associated with electrode surfaces,[70,71] etc. More importantly, drug release processes can be activated by the output signals controlled by biomarker signals processed through biocatalytic logic gates.[72−75] In the present majority gate/filter system, biocatalytically produced NADH was used to trigger polymer dissolution and a drug-mimicking release process. In order to achieve this, NADH was electrocatalytically oxidized on an

dx.doi.org/10.1021/jp504057u | J. Phys. Chem. B 2014, 118, 6775−6784

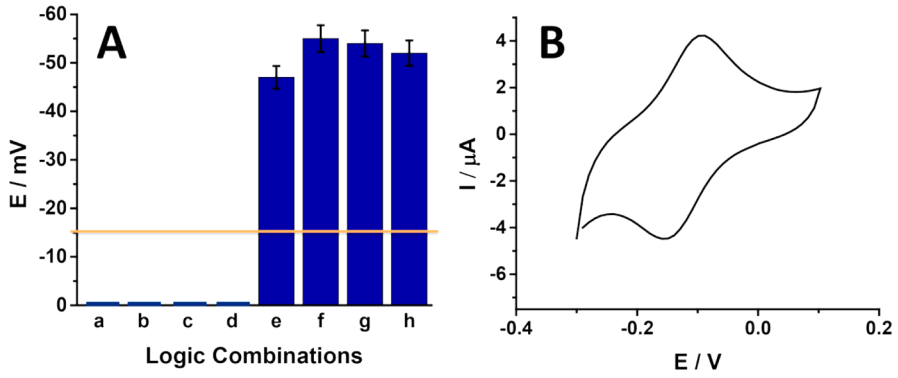

Figure 2. (A) Bar chart showing the potentials produced on the PQQ-modified electrode in the presence of NADH generated by the majority gate and processed through the filter system after application of the input signals in different combinations. The gate time for the potential measurements was 600 s. The input signal combinations were encoded in the following way: (a) **0**, **0**, **0**; (b) **0**, **1**, **0**; (c) **0**, **0**, **1**; (d) **1**, **0**, **0**; (e) **1**, **0**, **1**; (f) **0**, **1**, **1**; (g) **1**, **1**, **0**; (h) **1**, **1**, **1**. The input signals are shown in the flowing order: *A*, *B*, *C*. (B) Cyclic voltammogram obtained for the PQQ-modified electrode; pH = 7.4, potential scan rate 50 mV/s. Input signals are defined in Scheme 1 footnote.

electrode chemically modified with pyrroloquinoline quinone (PQQ),[76] resulting in the generation of a negative (reductive) potential. Figure 2A shows a bar chart of the potential changes on the PQQ-modified electrode corresponding to various combinations of the *A*, *B*, and *C* input signals processed through the majority gate/filter system. Since the potential value produced on the electrode upon NADH oxidation is logarithmically dependent on the NADH concentration (following the Nernst dependence), the spread of the output signals measured as potentials was significantly smaller compared to the optically measured signals which are linearly dependent on the NADH concentration. In the absence of NADH (output value **0** obtained at input combinations **0**, **0**, **0**; **0**, **0**, **1**; **0**, **1**, **0**; **1**, **0**, **0**) the potential on the PQQ electrode was close to 0 V. The potential value of ca. −50 mV was obtained for all input combinations (**0**, **1**, **1**; **1**, **0**, **1**; **1**, **1**, **0**; **1**, **1**, **1**) which results in the output value **1** according to the majority rule. The potential obtained in the presence of NADH is controlled by the redox potential value of PQQ, ca. −100 mV (Figure 2B), which operates as a catalyst.[76] The PQQ electrocatalytic electrode producing a reductive potential in the presence of NADH was then connected to another electrode modified with an alginate thin film containing embedded Fe_3O_4-magnetic-core/SiO_2-shell nanoparticles, ca. 50 nm, functionalized with a fluorescent dye (Rhodamine B) and HRP (NPs). The reductive potential produced on the PQQ electrode resulted in the electrochemically stimulated dissolution of the alginate film (Figure 3) and concomitant release of the NPs mimicking a drug-release process. Note that the NPs were functionalized with a fluorescent dye to enhance visualization of the polymer film dissolution. The process of electrochemical deposition of Fe^{3+}-cross-linked alginate and its electrochemical dissolution was studied in detail and reported elsewhere.[59] In summary, the alginate polymer was cross-linked by Fe^{3+} cations generated electrochemically to yield a gel on an electrode with NPs entrapped in the gel film upon its formation. The opposite process of gel dissolution and NP release proceeds when Fe^{3+} cations are reduced back to the Fe^{2+} state, which is unable to cross-link the alginate molecules. For an illustration of the different states of alginate, soluble and gel, in the presence of Fe^{2+} and Fe^{3+} cations, respectively, see Figure SI-1 in the Supporting Information. In our previous publications the Fe^{3+}-cross-linked alginate films were dissolved, and the entrapped species were released upon reduction of Fe^{3+}

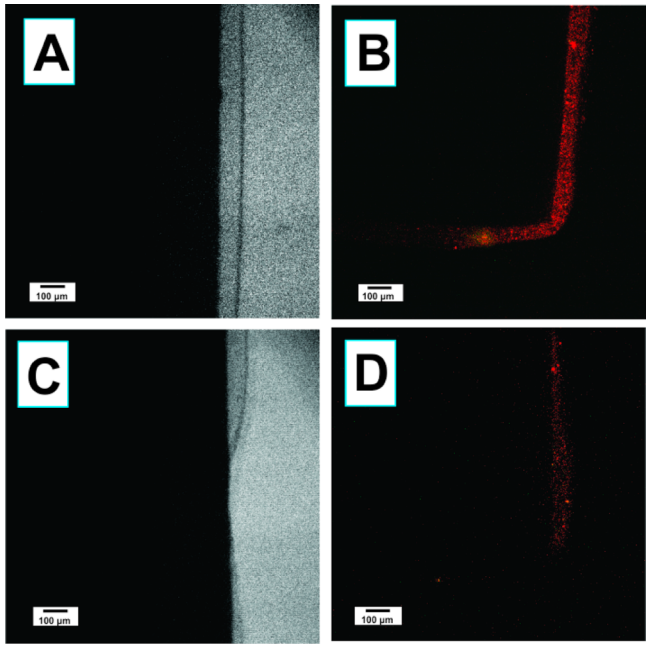

Figure 3. (A) Optical image of the boundary layer of the alginate film, including magnetic nanoparticles covered by a silica shell loaded with Rhodamina B dye, on a graphite electrode. (B) Fluorescent confocal microscopy image of the same alginate film. (C) Optical image of the boundary layer of the alginate film after its partial electrochemically induced dissolution for 30 min. (D) Fluorescent confocal microscopy image of boundary layer of the partially dissolved alginate film.

to Fe^{2+} cations by reductive potentials generated from a potentiostat[59,77] or produced *in situ* on biocatalytic electrodes.[78,79] In the present project the alginate dissolution and NP release was controlled by the majority rule implemented in the biocomputing system (Figure 4). The NPs released from the alginate film upon its electrochemical dissolution were analyzed by performing the standard enzymatic assay for HRP in the presence of TMB and H_2O_2 (see experimental details in the Supporting Information). The signal-controlled drug-mimicking release illustrated in this example can be used to increase the overall process robustness and to eliminate any false positive outputs since the final result (drug release) is controlled by the majority rule and activated only when at least two signals appear at their logic **1** values. The use of the

dx.doi.org/10.1021/jp504057u | *J. Phys. Chem. B* 2014, 118, 6775−6784

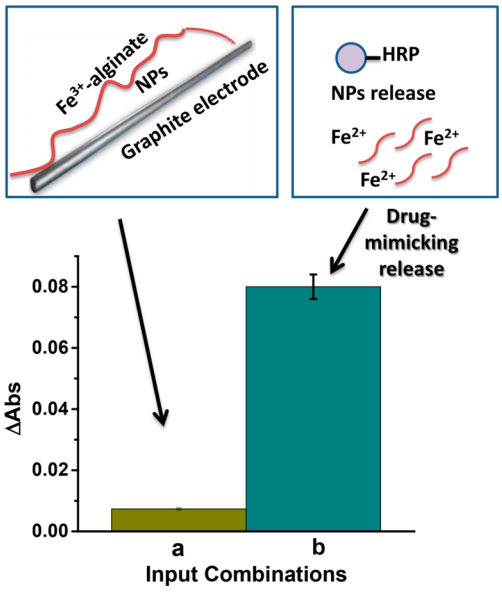

Figure 4. Bar chart showing the release of the NPs entrapped into the alginate thin film (b) comparing with the uncontrolled leakage of the NPs (a). The release process was induced by the input signals *A*, *B*, *C* applied in the following combinations: **0**, **1**, **1**; **1**, **0**, **1**; **1**, **1**, **0**; **1**, **1**, **1** and processed through the majority gate followed by the filter system. The leakage was observed when the following combinations of input signals were applied: **0**, **0**, **0**; **0**, **0**, **1**; **0**, **1**, **0**; **1**, **0**, **0**. Input signals are defined in Scheme 1 footnote.

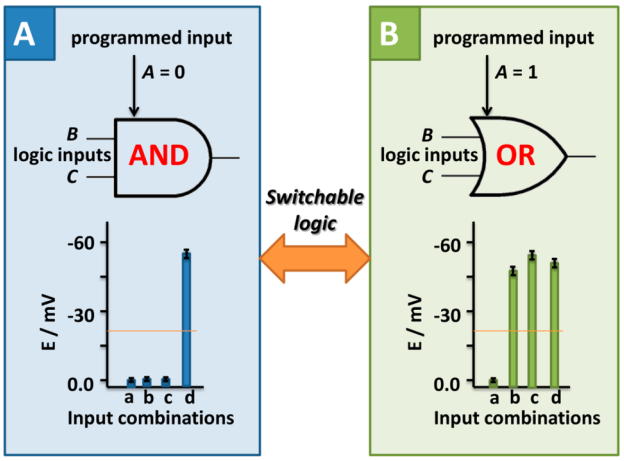

Figure 5. Switchable operation of the majority gate. The gate operates as AND or OR logic for inputs *B* and *C* when input *A* is reserved as the programming input and applied at the logic value **0** or **1**, respectively. The output signals are shown as the potentials generated on the PQQ-modified electrode in the presence of various combinations of input signals *B*, *C*: (a) **0**, **0**; (b) **0**, **1**; (c) **1**, **0**; (d) **1**, **1**. Input signals are defined in Scheme 1 footnote.

NPs with the magnetic core will allow their magneto-directed concentration in specific tissues in the future for *in vivo* applications.

A majority gate can be programmed to act as an OR gate or an AND gate by fixing any one of the three inputs as a programming input. If the programming input is **0**, the two remaining inputs perform the AND logic operation. If the programming input is **1**, the OR operation is performed on the other two inputs. In order to illustrate the switchable logic operation, we selected input *A* as the programmed input, while inputs *B* and *C* were used as logic inputs. Figure 5, A and B, shows operation of the AND and OR logic gates realized with the programming input *A* held at the logic values **0** and **1**, respectively. The output signal was defined as the potential measured on the PQQ-modified electrode, where the potential values of ca. −50 mV and ca. 0 mV were considered as logic values **1** and **0**, respectively. Note that the potential of ca. −50 mV (logic output **1**) was sufficient for the drug-mimicking release process described above, while the potential of ca. 0 mV (logic value **0**) preserved the alginate film and did not initiate the release process. Therefore, the logic operations resulting in drug release can be switched between AND/OR gates by fixing one of the three input signals (programmed input) at the logic value of **0** or **1** and using the other two input signals as variable logic signals. Obviously, the selection of the input for operating as the programmed input depends on the specific application. In other words, any input from three input signals can be selected as the programmed input for switching between AND and OR operations for two other inputs.

Enzyme-based logic systems can be extended to multistep biocatalytic cascades mimicking concatenated logic gates.[43,44] This was also illustrated in the present majority gate. Another reaction biocatalytically converting ethyl acetate (Et-Ac), input signal *C′*, to ethanol (Et-OH) in the presence of esterase (Est; E.C. 3.1.1.1), input signal *C″*, was added to produce Et-OH *in situ* for its reaction in the majority gate (Scheme 1A). It should be noted that for experimental convenience the enzyme Est was considered as a logically variable input signal, similar to the previously designed enzyme logic gates.[45,80] Logic values **0** for both additional input signals were defined as their absence, while their logic **1** values were experimentally optimized to activate the majority gate (note that all other components of the majority gate were also reoptimized; see Experimental Section for the details). The Et-OH production proceeded only in the presence of both input signals. In other words, when signals *C′* (Et-Ac) and *C″* (Est) were both applied at their logic **1** values, Et-OH was produced, thus mimicking an AND logic operation. The *in situ* produced Et-OH (the output signal of this AND gate) was used in substitution of the input signal *C* in the majority gate. Note that this input appeared only when inputs *C′* and *C″* both appeared at their **1** logic values. Overall, the concatenated AND-majority circuit generated output **1** in the following input *A*, *B*, *C′*, *C″* combinations: **1**, **1**, **1**, **1**; **1**, **1**, **1**, **0**; **1**, **1**, **0**, **1**; **0**, **1**, **1**, **1**; **1**, **0**, **1**, **1**; **1**, **1**, **0**, **0**. Figure 6 shows operation of the majority gate extended with the preceding AND gate and following filter system.

The 3-input minority gate was realized similarly to the majority gate described above with three reactions biocatalyzed by three NAD^+-dependent enzymes—malate dehydrogenase (MDH), diaphorase (Diaph), and lactic dehydrogenase (LDH)—operating in parallel (Scheme 3). The biocatalytic reactions were activated by input signals *A*, *B*, and *C* represented by the corresponding substrates: oxaloacetate (Oxacet), methylene blue (MB), and pyruvate (Pyr), respectively. Note that all the substrates were electron accepting species which induce the biocatalytic oxidation of NADH. This pathway is opposite comparing with the reactions used in the majority gate. Thus, all three reactions resulted in conversion of NADH to NAD^+ upon its biocatalytic oxidation and concomitant reduction of the substrate inputs. Logic values **1** for inputs *A*, *B*, and *C* were experimentally optimized and defined as 150, 105, and 100 μM, respectively, while the absence of the corresponding substrates was considered as logic

dx.doi.org/10.1021/jp504057u | J. Phys. Chem. B 2014, 118, 6775−6784

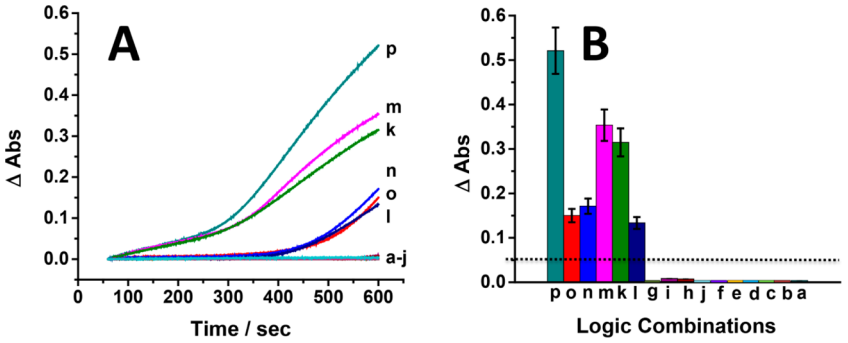

Figure 6. (A) Time-dependent absorbance changes corresponding to NADH production by the majority gate system integrated with the preceding AND gate and followed by the filter activated by various combinations of the input signals. (B) Bar chart showing the optical absorbance of NADH measured at λ = 340 nm at the gate time of 600 s for various combinations of the input signals. The input signal combinations were encoded in the following way: (a) **0**, **0**, **0**, **0**; (b) **1**, **0**, **0**, **0**; (c) **0**, **1**, **0**, **0**; (d) **0**, **0**, **1**, **0**; (e) **0**, **0**, **0**, **1**; (f) **1**, **0**, **1**, **0**; (g) **0**, **0**, **1**, **1**; (h) **0**, **1**, **1**, **0**; (i) **0**, **1**, **0**, **1**; (j) **1**, **0**, **0**, **1**; (k) **0**, **1**, **1**, **1**; (l) **1**, **1**, **0**, **0**; (m) **1**, **0**, **1**, **1**; (n) **1**, **1**, **0**, **1**; (o) **1**, **1**, **1**, **0**; (p) **1**, **1**, **1**, **1**. The input signals are shown in the flowing order: *A*, *B*, *C*′, *C*″. Input signals are defined in Scheme 1 footnote.

Scheme 3. Enzyme-Based 3-Input Minority Gate[a]

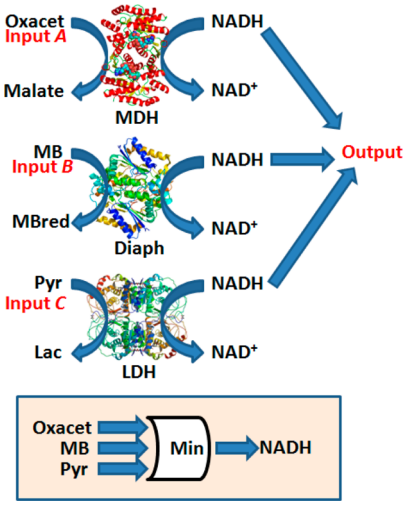

[a]The following abbreviations are used for the products of the biocatalytic reactions: MBred = reduced form of methylene blue, Lac = lactate. All other abbreviations are explained in the text. The enzyme images are given for the illustrating purposes only and may not correspond exactly to the used enzymes. Input signals *A*, *B*, and *C* are represented by oxaloacetate (Oxacet), methylene blue (MB), and pyruvate (Pyr), respectively.

value **0**. The output signal was defined as the optical absorbance of NADH (λ_{max} = 340 nm) (Figure 7A,B) or as the electrical potential produced on the PQQ-modified electrode in the presence of NADH (Figure 7C). As expected for the parallel operating biocatalytic reactions, the NADH consumption (conversion to NAD^+) was increased with the increasing number of reactions contributing to this process. In other words, in the absence of all substrates (meaning logic **0** value for all inputs), all three enzymes were mute, resulting in no consumption of NADH (Figure 7A, curve a). Applying any one of three input signals (Oxacet, MB, or Pyr) at its logic value **1** resulted in the activation of one biocatalytic reaction, resulting in NADH consumption and decreasing optical absorbance (Figure 7A, curves b–d). Note that the enzyme activities and input concentrations were optimized to result in similar rates of NADH consumption in all three biocatalytic processes. When two or all three inputs were applied at logic value **1**, the rate of NADH consumption was increased due to parallel operation of two or three biocatalytic reactions (Figure 7A, curves e–h). Figure 7B shows the optically measured output signals at the gate time of 600 s, where the low and high absorbance values correspond to logic **0** and **1** values, respectively. As expected for the minority function,[49] the logic output value **1** was obtained only if one or none of the input signals appeared at their logic **1** value. In the case where more than one input was applied at the logic **1** value, the system returned output **0**. However, the physical values corresponding to the logic **1** output were spread over a broad range of optical absorbance (Figure 7B). In order to consolidate the physical measure of the output signal, we measured the output signal as the potential electrocatalytically produced on the PQQ electrode in the presence of NADH. Similarly to the potential measurements upon operation of the majority gate (Figure 2A), the potentials measured in the present minority gate demonstrated small deviations from the average values—all potentials corresponding to the logic value **1** were measured close to −50 mV, while the potentials corresponding to the logic value **0** were ca. 0 mV (Figure 7C), thus significantly improving the outcome from the logic operation and resulting in smaller noise. As it was already explained for the majority gate, the improved output signals measured electrochemically can be explained by the logarithmic dependence of the measured potentials on the NADH concentration corresponding to the Nernst equation.

CONCLUSIONS AND PERSPECTIVES

Overall, the studied biocatalytic systems can be used to mimic the majority and minority logic functions; the quality of the output signals can be improved by adding a filter system and by measuring the electrochemical potentials, taking advantage of the logarithmic dependence on the concentration of the produced/consumed NADH. The enzyme-based logic systems can be extended to additional reaction steps mimicking various logic operations, thus allowing the integration of majority/minority gates into complex circuits of concatenated logic gates. The 3-input majority gate can be used for switching between AND/OR logic operations when one of the inputs is reserved as a command input and the two other inputs operate as variable logic inputs. This switchable logic operation will be particularly important in complex multifunctional logic networks, which are already designed for biomedical sensoric

dx.doi.org/10.1021/jp504057u | J. Phys. Chem. B 2014, 118, 6775–6784

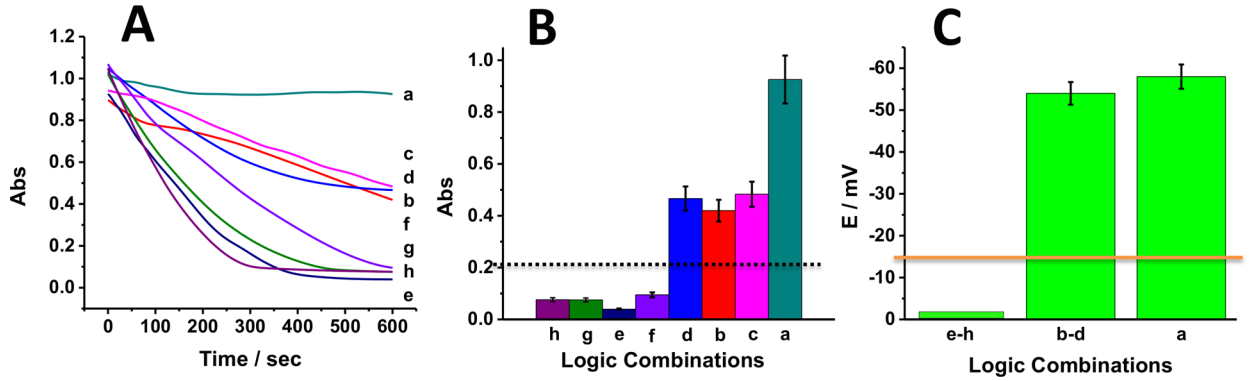

Figure 7. (A) Time-dependent absorbance changes corresponding to the NADH concentration upon operation of the minority gate activated by various combinations of the input signals. (B) Bar chart showing the optical absorbance of NADH measured at λ = 340 nm at the gate time of 600 s for various combinations of the input signals. (C) Bar chart showing the potentials produced on the PQQ-modified electrode in the presence of NADH upon operation of the minority gate after application of the input signals in different combinations. The gate time for the potential measurements was 600 s. The input signal combinations were encoded in the following way: (a) **0**, **0**, **0**; (b) **0**, **1**, **0**; (c) **0**, **0**, **1**; (d) **1**, **0**, **0**; (e) **1**, **0**, **1**; (f) **0**, **1**, **1**; (g) **1**, **1**, **0**; (h) **1**, **1**, **1**. The input signals are shown in the flowing order: *A*, *B*, *C*. Input signals are defined in Scheme 3 footnote.

operations.[45] The output signal generated by the majority/minority gates in the form of NADH can be used for various additional steps, including filter functions reducing noise and for the activation of chemical actuation, e.g., substance release or mimicking a drug release function. Future research in the area of enzyme-based logic systems, including those mimicking the majority/minority logic functions, should be concentrated on the use of flow devices with immobilized enzymes.[40] Technological realization of information processing systems in fluidic devices allows "clocking" (temporal control) and spatial separation of the various steps of multistage biochemical processes, thus providing novel options for their sophistication and functional flexibility.

■ ASSOCIATED CONTENT

Supporting Information

Experimental details: procedure for the NP preparation; illustrative picture of alginate cross-linking with iron cations and additional figures relating to the experimental characterization of the nanoparticles. This material is available free of charge via the Internet at http://pubs.acs.org.

■ AUTHOR INFORMATION

Corresponding Author

*Tel 1-315-268-4421, e-mail ekatz@clarkson.edu (E.K.).

Notes

The authors declare no competing financial interest.

■ ACKNOWLEDGMENTS

This work was supported by the NSF award # CBET-1066397 (Clarkson University) and DMR- 1426193 (University of Georgia).

■ REFERENCES

(1) Katz, E.; Privman, V. Enzyme-Based Logic Systems for Information Processing. *Chem. Soc. Rev.* **2010**, *39*, 1835−1857.
(2) *Molecular and Supramolecular Information Processing − From Molecular Switches to Unconventional Computing*; Katz, E., Ed.; Wiley-VCH: Weinheim, 2012.
(3) De Silva, A. P.; Uchiyama, S.; Vance, T. P.; Wannalerse, B. A Supramolecular Chemistry Basis for Molecular Logic and Computation. *Coord. Chem. Rev.* **2007**, *251*, 1623−1632.
(4) Szacilowski, K. Digital Information Processing in Molecular Systems. *Chem. Rev.* **2008**, *108*, 3481−3548.
(5) Credi, A. Molecules That Make Decisions. *Angew. Chem., Int. Ed.* **2007**, *46*, 5472−5475.
(6) Pischel, U. Chemical Approaches to Molecular Logic Elements for Addition and Subtraction. *Angew. Chem., Int. Ed.* **2007**, *46*, 4026−4040.
(7) Andréasson, J.; Pischel, U. Smart Molecules at Work—Mimicking Advanced Logic Operations. *Chem. Soc. Rev.* **2010**, *39*, 174−188.
(8) *Biomolecular Computing − From Logic Systems to Smart Sensors and Actuators*; Katz, E., Ed.; Wiley-VCH: Weinheim, 2012.
(9) Shapiro, E.; Gil, B. Biotechnology: Logic Goes in Vitro. *Nat. Nanotechnol.* **2007**, *2*, 84−85.
(10) Ashkenasy, G.; Ghadiri, M. R. Boolean Logic Functions of a Synthetic Peptide Network. *J. Am. Chem. Soc.* **2004**, *126*, 11140−11141.
(11) Stojanovic, M. N.; Stefanovic, D.; LaBean, T.; Yan, H. In *Bioelectronics: From Theory to Applications*; Willner, I., Katz, E., Eds.; Wiley-VCH: Weinheim, 2005; pp 427−455.
(12) Unger, R.; Moult, J. Towards Computing with Proteins. *Proteins* **2006**, *63*, 53−64.
(13) Ezziane, Z. DNA Computing: Applications and Challenges. *Nanotechnology* **2006**, *17*, R27−R39.
(14) Benenson, Y. Biocomputers: From Test Tubes to Live Cells. *Mol. Biosyst.* **2009**, *5*, 675−685.
(15) Stojanovic, M. N. Some Experiments and Directions in Molecular Computing and Robotics. *Isr. J. Chem.* **2011**, *51*, 99−105.
(16) Stojanovic, M. N.; Stefanovic, D. Chemistry at a Higher Level of Abstraction. *J. Comput. Theor. Nanosci.* **2011**, *8*, 434−440.
(17) Wang, J.; Katz, E. Digital Biosensors with Built-in Logic for Biomedical Applications − Biosensors Based on Biocomputing Concept. *Anal. Bioanal. Chem.* **2010**, *398*, 1591−1603.
(18) Wang, J.; Katz, E. Digital Biosensors with Built-in Logic for Biomedical Applications. *Isr. J. Chem.* **2011**, *51*, 141−150.
(19) Katz, E.; Wang, J.; Privman, M.; Halámek, J. Multianalyte Digital Enzyme Biosensors with Built-in Boolean Logic. *Anal. Chem.* **2012**, *84*, 5463−5469.
(20) Mailloux, S.; Halámek, J.; Halámková, L.; Tokarev, A.; Minko, S.; Katz, E. Biomolecular Release Triggered by Glucose Input − Bioelectronic coupling of Sensing and Actuating Systems. *Chem. Commun.* **2013**, *49*, 4755−4757.
(21) Privman, M.; Tam, T. K.; Bocharova, V.; Halámek, J.; Wang, J.; Katz, E. Responsive Interface Switchable by Logically Processed Physiological Signals − Towards "Smart" Actuators for Signal Amplification and Drug Delivery. *ACS Appl. Mater. Interfaces* **2011**, *3*, 1620−1623.

(22) Strack, G.; Bocharova, V.; Arugula, M. A.; Pita, M.; Halámek, J.; Katz, E. Artificial Muscle Reversibly Controlled by Enzyme Reactions. *J. Phys. Chem. Lett.* **2010**, *1*, 839−843.
(23) Katz, E.; Wang, J. Enzyme-Logic Digital Biosensors for Biomedical Applications. In *Biomolecular Information Processing − From Logic Systems to Smart Sensors and Actuators*; Katz, E., Ed.; Wiley-VCH: Weinheim, 2012; Chapter 5, pp 81−101.
(24) Melnikov, D.; Strack, G.; Zhou, J.; Windmiller, J. R.; Halámek, J.; Bocharova, V.; Chuang, M.-C.; Santhosh, P.; Privman, V.; Wang, J.; Katz, E. Enzymatic AND Logic Gates Operated Under Conditions Characteristic of Biomedical Applications. *J. Phys. Chem. B* **2010**, *114*, 12166−12174.
(25) May, E. E.; Dolan, P. L.; Crozier, P. S.; Brozik, S.; Manginell, M. Towards De Novo Design of Deoxyribozyme Biosensors for GMO Detection. *IEEE Sens. J.* **2008**, *8*, 1011−1019.
(26) von Maltzahn, G.; Harris, T. J.; Park, J.-H.; Min, D.-H.; Schmidt, A. J.; Sailor, M. J.; Bhatia, S. N. Nanoparticle Self-Assembly Gated by Logical Proteolytic Triggers. *J. Am. Chem. Soc.* **2007**, *129*, 6064−6065.
(27) Kahan, M.; Gil, B.; Adar, R.; Shapiro, E. Towards Molecular Computers that Operate in a Biological Environment. *Physica D* **2008**, *237*, 1165−1172.
(28) Rinaudo, K.; Bleris, L.; Maddamsetti, R.; Subramanian, S.; Weiss, R.; Benenson, Y. A Universal RNAi-Based Logic Evaluator That Operates in Mammalian Cells. *Nat. Biotechnol.* **2007**, *25*, 795−801.
(29) Gdor, E.; Katz, E.; Mandler, D. Biomolecular AND Logic Gate Based on Immobilized Enzymes with Precise Spatial Separation Controlled by Electrochemical Scanning Microscopy. *J. Phys. Chem. B* **2013**, *117*, 16058−16065.
(30) Bakshi, S.; Zavalov, O.; Halámek, J.; Privman, V.; Katz, E. Modularity of Biochemical Filtering for Inducing Sigmoid Response in Both Inputs in an Enzymatic AND Gate. *J. Phys. Chem. B* **2013**, *117*, 9857−9865.
(31) Privman, V.; Fratto, B. E.; Zavalov, O.; Halámek, J.; Katz, E. Enzymatic AND Logic Gate with Sigmoid Response Induced by Photochemically Controlled Oxidation of the Output. *J. Phys. Chem. B* **2013**, *117*, 7559−7568.
(32) Halámek, J.; Zavalov, O.; Halámková, L.; Korkmaz, S.; Privman, V.; Katz, E. Enzyme-Based Logic Analysis of Biomarkers at Physiological Concentrations: AND Gate with Double-Sigmoid "Filter" Response. *J. Phys. Chem. B* **2012**, *116*, 4457−4464.
(33) Privman, V.; Pedrosa, V.; Melnikov, D.; Pita, M.; Simonian, A.; Katz, E. Enzymatic AND-Gate Based on Electrode-Immobilized Glucose-6-phosphate Dehydrogenase: Towards Digital Biosensors and Biochemical Logic Systems with Low Noise. *Biosens. Bioelectron.* **2009**, *25*, 695−701.
(34) Strack, G.; Pita, M.; Ornatska, M.; Katz, E. Boolean Logic Gates Using Enzymes as Input Signals. *ChemBioChem* **2008**, *9*, 1260−1266.
(35) Baron, R.; Lioubashevski, O.; Katz, E.; Niazov, T.; Willner, I. Two Coupled Enzymes Perform in Parallel the "AND" and "InhibAND" Logic Gates Operations. *Org. Biomol. Chem.* **2006**, *4*, 989−991.
(36) Baron, R.; Lioubashevski, O.; Katz, E.; Niazov, T.; Willner, I. Logic Gates and Elementary Computing by Enzymes. *J. Phys. Chem. A* **2006**, *110*, 8548−8553.
(37) Zavalov, O.; Bocharova, V.; Privman, V.; Katz, E. Enzyme-Based Logic: OR Gate with Double-Sigmoid Filter Response. *J. Phys. Chem. B* **2012**, *116*, 9683−9689.
(38) Zhou, N.; Windmiller, J. R.; Valdés Ramírez, G.; Zhou, M.; Halámek, J.; Katz, E.; Wang, J. Enzyme-Based NAND Gate for Rapid Electrochemical Screening of Traumatic Brain Injury in Serum. *Anal. Chim. Acta* **2011**, *703*, 94−100.
(39) Zhou, J.; Arugula, M. A.; Halámek, J.; Pita, M.; Katz, E. Enzyme-Based NAND and NOR Logic Gates with Modular Design. *J. Phys. Chem. B* **2009**, *113*, 16065−16070.
(40) Moseley, F.; Halámek, J.; Kramer, F.; Poghossian, A.; Schöning, M. J.; Katz, E. Enzyme-Based Reversible CNOT Logic Gate Realized in a Flow System. *Analyst* **2014**, *139*, 1839−1842.
(41) Halámek, J.; Bocharova, V.; Arugula, M. A.; Strack, G.; Privman, V.; Katz, E. Realization and Properties of Biochemical-Computing Biocatalytic XOR Gate Based on Enzyme Inhibition by a Substrate. *J. Phys. Chem. B* **2011**, *115*, 9838−9845.
(42) Privman, V.; Zhou, J.; Halámek, J.; Katz, E. Realization and Properties of Biochemical-Computing Biocatalytic XOR Gate Based on Signal Change. *J. Phys. Chem. B* **2010**, *114*, 13601−13608.
(43) Privman, V.; Arugula, M. A.; Halámek, J.; Pita, M.; Katz, E. Network Analysis of Biochemical Logic for Noise Reduction and Stability: A System of Three Coupled Enzymatic AND Gates. *J. Phys. Chem. B* **2009**, *113*, 5301−5310.
(44) Privman, V.; Zavalov, O.; Halámková, L.; Moseley, F.; Halámek, J.; Katz, E. Networked Enzymatic Logic Gates with Filtering: New Theoretical Modeling Expressions and Their Experimental Application. *J. Phys. Chem. B* **2013**, *117*, 14928−14939.
(45) Halámek, J.; Bocharova, V.; Chinnapareddy, S.; Windmiller, J. R.; Strack, G.; Chuang, M.-C.; Zhou, J.; Santhosh, P.; Ramirez, G. V.; Arugula, M. A.; et al. Multi-Enzyme Logic Network Architectures for Assessing Injuries: Digital Processing of Biomarkers. *Mol. Biosyst.* **2010**, *6*, 2554−2560.
(46) Halámek, J.; Windmiller, J. R.; Zhou, J.; Chuang, M.-C.; Santhosh, P.; Strack, G.; Arugula, M. A.; Chinnapareddy, S.; Bocharova, V.; Wang, J.; et al. Multiplexing of Injury Codes for the Parallel Operation of Enzyme Logic Gates. *Analyst* **2010**, *135*, 2249−2259.
(47) MacVittie, K.; Halámek, J.; Privman, V.; Katz, E. A Bioinspired Associative Memory System Based on Enzymatic Cascades. *Chem. Commun.* **2013**, *49*, 6962−6964.
(48) Bocharova, V.; MacVittie, K.; Chinnapareddy, S.; Halámek, J.; Privman, V.; Katz, E. Realization of Associative Memory in an Enzymatic Process: Toward Biomolecular Networks with Learning and Unlearning Functionalities. *J. Phys. Chem. Lett.* **2012**, *3*, 1234−1237.
(49) Zhang, R.; Gupta, P.; Jha, N. K. Majority and Minority Network Synthesis with Application to QCA-, SET-, and TPL-Baced Nanotechnologies. *IEEE Trans. Comput.-Aided Des. Integr. Circuits Syst.* **2007**, *26*, 1233−1245.
(50) Goldmann, M.; Karpinski, M. Simulating Threshold Circuits by Majority Circuits. *SIAM J. Comput.* **1998**, *27*, 230−246.
(51) Yang, X.; Cai, L.; Kang, Q. Magnetic Quantum Cellular Automata-Based Logic Computation Structure: A Full-Adder Study. *J. Comput. Theor. Nanosci.* **2012**, *9*, 621−625.
(52) Imre, A.; Csaba, G.; Ji, L.; Orlov, A.; Bernstein, G. H.; Porod, W. Majority Logic Gate for Magnetic Quantum-Dot Cellular Automata. *Science* **2006**, *311*, 205−208.
(53) Stroud, C. E. Reliability of Majority Voting Based VLSI Fault-Tolerant Circuits. *IEEE Trans. VLSI Syst.* **1994**, *2*, 516−521.
(54) Yang, G.; Hung, W. N. N.; Song, X.; Perkowski, M. Majority-Based Reversible Logic Gates. *Theor. Comput. Sci.* **2005**, *334*, 259−274.
(55) Li, W.; Yang, Y.; Yan, H.; Liu, Y. Three-Input Majority Logic Gate and Multiple Input Logic Circuit Based on DNA Strand Displacement. *Nano Lett.* **2013**, *13*, 2980−2988.
(56) Zhu, J.; Zhang, L.; Dong, S.; Wang, E. Four-Way Junction-Driven DNA Strand Displacement and Its Application in Building Majority Logic Circuit. *ACS Nano* **2013**, *7*, 10211−10217.
(57) Bumb, A.; Brechbiel, M. W.; Choyke, P. L.; Fugger, L.; Eggeman, A.; Prabhakaran, D.; Hutchinson, J.; Dobson, P. J. Synthesis and Characterization of Ultra-Small Superparamagnetic Iron Oxide Nanoparticles Thinly Coated with Silica. *Nanotechnology* **2008**, *19*, art. #335601.
(58) Kariuki, J. K. An Electrochemical and Spectroscopic Characterization of Pencil Graphite Electrodes. *J. Electrochem. Soc.* **2012**, *159*, H747−H751.
(59) Jin, Z.; Güven, G.; Bocharova, V.; Halámek, J.; Tokarev, I.; Minko, S.; Melman, A.; Mandler, D.; Katz, E. Electrochemically Controlled Drug-Mimicking Protein Release from Iron-Alginate Thin-Films Associated with an Electrode. *ACS Appl. Mater. Interfaces* **2012**, *4*, 466−475.
(60) Katz, E.; Schlereth, D. D.; Schmidt, H.-L. Electrochemical Study of Pyrroloquinoline Quinone Covalently Immobilized as Monolayer

onto a Cystamine Modified Gold Electrode. *J. Electroanal. Chem.* **1994**, *367*, 59−70.
(61) Dawson, R. B. *Data for Biochemical Research*, 3rd ed.; Clarendon Press: Oxford, 1985; p 122.
(62) Silverstein, E.; Sulebele, G. Catalytic Mechanism of Pig Heart Mitochondrial Malate Dehydrogenase Studied by Kinetics at Equilibrium. *Biochemistry* **1969**, *8*, 2543−2550.
(63) Mailloux, S.; Zavalov, O.; Guz, N.; Katz, E.; Bocharova, V. Enzymatic Filter for Improved Separation of Output Signals in Enzyme Logic Systems Towards 'Sense and Treat' Medicine. *Biomater. Sci.* **2014**, *2*, 184−191.
(64) Bocharova, V.; Katz, E. Switchable Electrode Interfaces Controlled by Physical, Chemical and Biological Signals. *Chem. Rec.* **2012**, *12*, 114−130.
(65) Pita, M.; Minko, S.; Katz, E. Enzyme-Based Logic Systems and Their Applications for Novel Multi-Signal-Responsive Materials. *J. Mater. Sci.: Mater. Med.* **2009**, *20*, 457−462.
(66) Katz, E.; Bocharova, V.; Privman, M. Electronic Interfaces Switchable by Logically Processed Multiple Biochemical and Physiological Signals. *J. Mater. Chem.* **2012**, *22*, 8171−8178.
(67) Motornov, M.; Zhou, J.; Pita, M.; Gopishetty, V.; Tokarev, I.; Katz, E.; Minko, S. "Chemical Transformers" from Nanoparticle Ensembles Operated with Logic. *Nano Lett.* **2008**, *8*, 2993−2997.
(68) Motornov, M.; Zhou, J.; Pita, M.; Tokarev, I.; Gopishetty, V.; Katz, E.; Minko, S. An Integrated Multifunctional Nanosystem from Command Nanoparticles and Enzymes. *Small* **2009**, *5*, 817−820.
(69) Tokarev, I.; Gopishetty, V.; Zhou, J.; Pita, M.; Motornov, M.; Katz, E.; Minko, S. Stimuli-Responsive Hydrogel Membranes Coupled with Biocatalytic Processes. *ACS Appl. Mater. Interfaces* **2009**, *1*, 532−536.
(70) Zhou, J.; Tam, T. K.; Pita, M.; Ornatska, M.; Minko, S.; Katz, E. Bioelectrocatylic System Coupled with Enzyme-Based Biocomputing Ensembles Performing Boolean Logic Operations: Approaching "Smart" Physiologically Controlled Biointerfaces. *ACS Appl. Mater. Interfaces* **2009**, *1*, 144−149.
(71) Privman, M.; Tam, T. K.; Bocharova, V.; Halámek, J.; Wang, J.; Katz, E. Responsive Interface Switchable by Logically Processed Physiological Signals − Towards "Smart" Actuators for Signal Amplification and Drug Delivery. *ACS Appl. Mater. Interfaces* **2011**, *3*, 1620−1623.
(72) Bocharova, V.; Zavalov, O.; MacVittie, K.; Arugula, M. A.; Guz, N. V.; Dokukin, M. E.; Halámek, J.; Sokolov, I.; Privman, V.; Katz, E. Biochemical Logic Approach to Biomarker-Activated Drug Release. *J. Mater. Chem.* **2012**, *22*, 19709−19717.
(73) Mailloux, S.; Zavalov, O.; Guz, N.; Katz, E.; Bocharova, V. Enzymatic Filter for Improved Separation of Output Signals in Enzyme Logic Systems Towards 'Sense and Treat' Medicin. *Biomater. Sci.* **2014**, *2*, 184−191.
(74) Mailloux, S.; Halámek, J.; Katz, E. Model System for Targeted Drug Release Triggered by Biomolecular Signals Logically Processed Through Enzyme Logic Networks. *Analyst* **2014**, *139*, 982−986.
(75) Mailloux, S.; Halámek, J.; Halámková, L.; Tokarev, A.; Minko, S.; Katz, E. Biomolecular Release Triggered by Glucose Input − Bioelectronic Coupling of Sensing and Actuating Systems. *Chem. Commun.* **2013**, *49*, 4755−4757.
(76) Katz, E.; Lötzbeyer, T.; Schlereth, D. D.; Schuhmann, W.; Schmidt, H.-L. Electrocatalytic Oxidation of Reduced Nicotinamide Coenzymes at Gold and Platinum Electrode Surfaces Modified with a Monolayer of Pyrroloquinoline Quinone. Effect of Ca^{2+} Cations. *J. Electroanal. Chem.* **1994**, *373*, 189−200.
(77) Jin, Z.; Harvey, A. M.; Mailloux, S.; Halámek, J.; Bocharova, V.; Twiss, M. R.; Katz, E. Electrochemically Stimulated Release of Lysozyme from Alginate Matrix Cross-Linked with Iron Cations. *J. Mater. Chem.* **2012**, *22*, 19523−19528.
(78) Mailloux, S.; Halámek, J.; Katz, E. Model System for Targeted Drug Release Triggered by Biomolecular Signals Logically Processed Through Enzyme Logic Networks. *Analyst* **2014**, *139*, 982−986.
(79) Mailloux, S.; Halámek, J.; Halámková, J.; Tokarev, A.; Minko, S.; Katz, E. Biomolecular Release Triggered by Glucose Input − Bioelectronic Coupling of Sensing and Actuating Systems. *Chem. Commun.* **2013**, *49*, 4755−4757.
(80) Strack, G.; Pita, M.; Ornatska, M.; Katz, E. Boolean Logic Gates Using Enzymes as Input Signals. *ChemBioChem* **2008**, *9*, 1260−1266.